Optimal Fault-Tolerant Control of Six-Phase Induction Motor Drives with Parallel Converters

M.J. Duran, I. Gonzalez, M. Bermudez, F. Barrero, *Senior Member*, *IEEE*, H. Guzman, M.R. Arahal, *Member*

***Abstract*– Multiphase drives and parallel converters have been recently proposed in low-voltage high-power applications. The fault-tolerant capability provided by multiphase drives is then extended with parallel converters, increasing their suitability for safety-critical and renewable uses. This advantageous feature, compared to standard three-phase drives, has been analyzed in the event of open-phase faults. However, when using parallel converters, a converter fault does not necessarily imply an open-phase condition, but usually just a limited phase current capability. This work analyzes the fault-tolerant capability of six-phase drives with parallel converter supply. Different scenarios considering up to three faults for single and two neutral configurations are examined, optimizing off-line the post-fault currents and modifying accordingly the control strategies. Experimental results confirm the smooth transition from pre- to post-fault situations and the enhanced post-fault torque capability.**

***Index Terms*– Multiphase drives, Fault-tolerance, Field oriented control.**

NOMENCLATURE

BTB	Back-to-back.
FOC	Field oriented control.
IM	Induction machine.
PM	Permanent Magnet machine.
PR	Resonant controller.
PWM	Pulse width modulation.
VSC	Voltage source converter.
VSD	Vector space decomposition.
$e_{d,q}$	Decoupling terms.
$i^*_{a1,b1,c1,a2,b2,c2}$	Stator reference currents.
$I_{a1,b1,c1,a2,b2,c2}$	Phasor's amplitude of stator currents.
$i_{\alpha,\beta s}$	Stator currents in the α-β subspace.
$I_{\alpha,\beta}$	Phasor's amplitude of the α-β currents.
$i_{x,ys}$	Stator currents in the x-y subspace.
$I_{x,y}$	Phasor's amplitude of the x-y currents.
$i_{0_+,0_-s}$	Stator currents in the 0_+0_- subspace.
$I_{0_+,0_-}$	Phasor's amplitude of the 0_+0_- currents.
$i_{\alpha,\beta r}$	Rotor currents in the α-β subspace.
$i_{d,q}$	Direct and quadature currents.
$i^*_{d,q}$	Direct and quadrature reference currents.
I_j	rms currents in the healthy phases.
I_k	rms currents in the faulted phases.
I_n	Rated rms current.
$v_{\alpha,\beta s}$	Stator voltages in the α-β subspace.
$v_{x,ys}$	Stator voltages in the x-y subspace.
$v^*_{d,q}$	Direct and quadrature reference voltages.
$v^*_{a1,b1,c1,a2,b2,c2}$	Stator phase reference voltages.
$v_{0_+,0_-s}$	Stator voltages in the 0_+0_- subspace.
L_{ls}	Stator leakage inductance.
L_{lr}	Rotor leakage inductance.
L_s	Stator inductance.
L_r	Rotor inductance.
M	Mutual inductance.
p	Number of pole pairs.
R_s	Stator resistance.
R_r	Rotor resistance.
T_e	Electrical torque.
T_r	Rotor time constant.
$\varphi_{a1,b1,c1,a2,b2,c2}$	Phasor's angle of the stator currents.
$\varphi_{\alpha,\beta}$	Phasor's angle of the α-β currents.
$\varphi_{x,y}$	Phasor's angle of the x-y currents.
$\varphi_{0_+,0_-}$	Phasor's angle of the 0_+0_- currents.
θ_s	Angle of the rotating reference frame.
ω	Measured speed.
ω_r	Rotor electrical speed.

Manuscript received February 5, 2015; revised May 13, 2015; accepted June 13, 2015.

This work was supported by the Spanish Ministry of Science and Innovation under Projects ENE2014-52536-C2-1-R and DPI2013-44278-R, and the Junta de Andalucía under Project P11-TEP-7555.

M.J. Duran and H. Guzman are with the Department of Electrical Engineering at the University of Malaga, Spain, e-mail: mjduran@uma.es.

I. Gonzalez-Prieto, M. Bermudez, F. Barrero and M.R. Arahal are with the Department of Electronic Engineering and Automatic Control at the University of Seville, Spain, e-mail: fbarrero@us.es.

I. INTRODUCTION

Fault tolerance is a desirable feature of electrical drives that is especially appreciated in safety-critical applications such as aerospace or military naval drives [1-3]. In such cases, the inherent redundancy provided by multiphase systems allows the fault-tolerant operation of the drive with no additional hardware. Industry funded projects are thus promoting the development of multiphase machines in 'more electric aircraft' actuators [4]. In other applications the post-fault operation is not mandatory but it is also highly appreciated because of the economic benefits that are derived from the continuous operation of the drive. An example of this situation can be found in offshore wind energy industry, where the shut-down of a generating unit can be prolonged depending on the weather conditions [5]. Regardless of the application, the fault tolerant capability of multiphase drives has an unquestionable interest for industry and it is thus a focus of recent research.

Even though the use of multiphase drives requires a multiphase power supply, the increasing level of rated power in low-voltage applications and the limited current capability of IGBT-based converters inevitably leads to the use of multiple three-phase voltage source converters (VSCs) [6]. In this case, the use of electrical machines with multiple sets of three-phase windings appears as a natural solution that simultaneously provides a reduction in the per phase current ratings and an increment in the fault tolerant capability.

Industrial examples of multiphase drives with multiple sets of three phase windings supplied from three-phase converters are the 1.1 MW nine-phase drive used in a traction application for the world's tallest elevator test tower [7] and the 5 MW twelve-phase wind energy conversion system [8].

In this scenario of increasing interest on multiphase drives for high-power low-voltage applications, an intense research has been conducted to improve their fault tolerant operation. The main research lines found in the existing literature are: *i*) the development of fault detection techniques [9-10], *ii*) the optimization of post-fault current references to obtain maximum torque and/or minimum copper losses [11-13] and *iii*) the development of control strategies to adequately handle the asymmetrical post-fault situation [14-20]. These works mainly focus on the fault tolerant operation in the event of open-circuit faults. Short-circuit faults have also been addressed [21-22], but the post-fault operation is only allowed with a specific design of the machine (typically with high self-inductances and isolation between the different sets of three-phase windings). The previous studies in literature have mainly covered five- and six-phase machines, either induction or permanent magnet (PM). Although initial works considered machines with distributed windings and negligible spatial harmonics, recent ones deal with concentrated windings, using multi-frequency supply to enhance the fault-tolerant characteristic and the torque production of the multiphase drive [12,23-24]. Different winding connections have also been explored for five-phase machines, comparing the performance of star, pentagon and pentacle connections of stator windings [17-18,25].

In spite of the abundant contributions in the field, a common feature of the aforementioned works is the consideration of topologies where the stator windings are supplied from single VSCs, which in turn leads to open phase/line faults. Alternatively, if the multiphase machine is supplied from parallel VSCs, the situation differs because converter faults do not entail an open-phase situation. Conversely, the phase involved in the fault can still draw current from the healthy parallel converter. This situation has only been addressed in [26-27] for hybrid series/parallel connection of the converters. However, the use of independent dc-links for each set of three-phase windings forces the currents of the faulted set to be balanced in order to prevent dc-link voltage oscillations [28].

This work explores for the first time the fault tolerant capability of six-phase induction motor drives supplied from parallel converters connected to a common dc-link. The main difference with the case of independent dc-links [7-8,29] is that the currents of the faulted set of three-phase windings do not need to be balanced. This additional degree of freedom improves the fault tolerance of the drive, achieving higher post-fault torque/power. The analysis includes: *i*) the off-line optimization of the post-fault phase currents, *ii*) the derivation of the post-fault *x-y* currents and *iii*) the proposal of suitable control schemes for the different types of faults. These contributions are developed considering single and two neutrals. From the point of view of the fault tolerance, it is well-known that the additional degree of freedom using single neutral connection reduces the post-fault derating [29]. However, the usual choice in pre-fault situation is to operate with two neutrals in order to increase the dc-link voltage utilization and prevent the flow of zero sequence currents.

The paper is structured as follows. Section II describes the six-phase induction motor drive with parallel converter supply. Current references to maximize torque production in post-fault operation are obtained in section III. Section IV presents some control schemes proposed for different fault types. Experimental results that confirm the capability of the suggested control schemes are shown in section V, where it is demonstrated the tracking ability of the stator current to follow the current references obtained in section III. The main conclusions are finally summarized in section VI.

II. Six-phase Induction Motor Drives with Parallel Converters

The six-phase induction motor drive considered in what follows includes an asymmetrical six-phase machine with two sets of three-phase windings ($a_1b_1c_1$ and $a_2b_2c_2$) that are spatially shifted 30º and are supplied from two-level three-phase VSCs (Fig. 1). In full-power energy conversion systems with bidirectional power flow, the dc-links of the two three-phase VSCs can be connected in series [26-28], parallel [30] or remain independent [7-8].

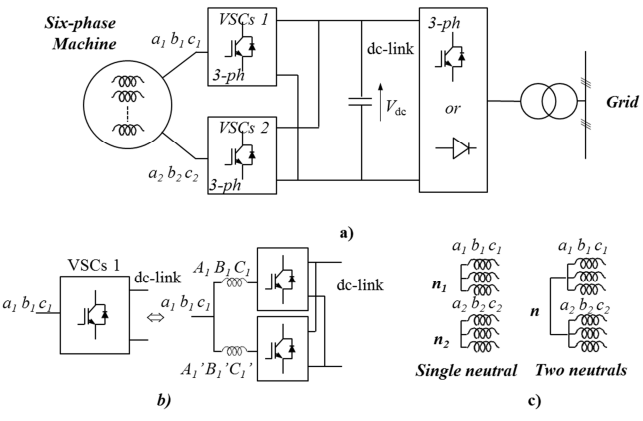

Fig. 1. Six-phase induction motor drive topology (a), parallel connection of VSCs (b) and single and two neutrals connection (c).

The series connection elevates the dc-link voltage allowing medium voltage on the grid-side, and this feature is interesting to obtain transformerless generation [30-31]. The use of independent dc-links in back-to-back (BTB) modules provides simple fault-tolerant capability overriding the faulted BTB set and operating in 'single VSC' mode [29]. However, the most common arrangement in motor drives is the parallel connection of the two VSCs, as shown in Fig. 1a. The grid-side connection can be performed with diode rectifiers or active rectifiers if regenerative braking is needed [7]. The parallel connection of single VSCs to a common dc-link improves the fault-tolerant capability because the motor can operate with the remaining five healthy phases instead of the 'single VSC' mode that only achieves 50% of the rated α-β currents. This mode of operation has been investigated in several works showing that post-fault operation is feasible provided that the current references and control scheme are adequately modified.

Nevertheless, the use of two VSCs to drive the six-phase machine can be insufficient in high-power low-voltage applications with high per-phase currents [6]. In such cases, similarly to the standard procedure in three-phase drives, the two VSCs supplying windings $a_1b_1c_1$ and $a_2b_2c_2$ can be replaced by modules with two converters in parallel (Fig. 1b). For the purpose of the discussion that follows, it is assumed that the set of windings $a_1b_1c_1$ is connected to VSCs $A_1B_1C_1$ and $A_1'B_1'C_1'$ (collectively termed as VSCs1), and the set of windings $a_2b_2c_2$ is connected to VSCs $A_2B_2C_2$ and $A_2'B_2'C_2'$ (collectively termed as VSCs2). Assuming without lack of generality that leg-A_1' of the VSCs1 is faulted, phase a_1 can still be supplied with leg-A_1 of VSCs1. In this case the converter fault does not imply an open-phase as in [29]. Instead, the maximum current of the faulted phase is reduced to half the rated value (i.e. $I_n/2$). The other five phases remain healthy maintaining the capability to supply rated current (I_n).

It follows that the drive operates in post-fault situation with six phases but in an asymmetrical manner. It must be highlighted that the use of a single dc-link eliminates the constraint of balanced operation in the faulted set of three-phase windings. Topologies with independent dc-links [7-8,26-29] require constant power in each individual dc-link to avoid voltage oscillations, and this implies that currents in phases b_1 and c_1 need to be limited to $I_n/2$. On the contrary, in the topology with a single dc-link shown in Fig. 1, only the total power needs to remain constant and this allows increasing the currents in phases b_1 and c_1 up to I_n.

In the case of parallel supply with four three-phase VSCs shown in Fig. 1 one may consider different fault scenarios. This work considers the scenarios with up to three simultaneous faults in either VSCs1 and VSCs2, excluding the cases when two faults affect the same phase (e.g. fault in leg A_1' and A_1) because this would imply an open-phase of phase a_1, and this situation has been covered in [29]. In general, the post-fault situation must satisfy the restrictions:

$$\begin{aligned} &I_k \le \frac{I_n}{2} \;\; \forall k \in \{Faulted\ phases\} \\ &I_j \le I_n \;\; \forall j \in \{Healthy\ phases\} \end{aligned} \tag{1}$$

where I_n is the rated rms current, I_k are the rms currents in the faulted phases and I_j are the rms currents in the remaining healthy phases. The constraints of (1) ensure that the drive operates within its thermal limit after the fault. It is also possible to allow post-fault currents over the rated value maintaining the pre-fault copper losses [13,32]. Although this less conservative criterion reduces the systems derating, care must be taken to ensure that hot spots do not appear in the machine. This work follows the criterion of (1) which is on the safe side.

Even though the thermal restrictions are imposed to phase currents (1), the control of the machine is typically done in vector space decomposition (VSD) variables obtained from the generalized Clarke transformation:

$$[T_6] = \frac{1}{\sqrt{3}}\begin{bmatrix} 1 & -1/2 & -1/2 & \sqrt{3}/2 & -\sqrt{3}/2 & 0 \\ 0 & \sqrt{3}/2 & -\sqrt{3}/2 & 1/2 & 1/2 & -1 \\ 1 & -1/2 & -1/2 & -\sqrt{3}/2 & \sqrt{3}/2 & 0 \\ 0 & -\sqrt{3}/2 & \sqrt{3}/2 & 1/2 & 1/2 & -1 \\ 1 & 1 & 1 & 0 & 0 & 0 \\ 0 & 0 & 0 & 1 & 1 & 1 \end{bmatrix} \tag{2}$$

Applying the transformation of (2) to the phase variable model [1-2], the machine model is decomposed into α-β, x-y and 0_+-0_- subspaces:

$$\begin{aligned} v_{\alpha s} &= \left(R_s + L_s \cdot \frac{d}{dt}\right) \cdot i_{\alpha s} + M \cdot \frac{di_{\alpha r}}{dt} \\ v_{\beta s} &= \left(R_s + L_s \cdot \frac{d}{dt}\right) \cdot i_{\beta s} + M \cdot \frac{di_{\beta r}}{dt} \\ v_{xs} &= \left(R_s + L_s \cdot \frac{d}{dt}\right) \cdot i_{xs} \\ v_{ys} &= \left(R_s + L_s \cdot \frac{d}{dt}\right) \cdot i_{ys} \\ v_{0+s} &= \left(R_s + L_s \cdot \frac{d}{dt}\right) \cdot i_{0+s} \\ v_{0-s} &= \left(R_s + L_s \cdot \frac{d}{dt}\right) \cdot i_{0-s} \\ 0 &= \left(R_r + L_r \cdot \frac{d}{dt}\right) \cdot i_{\alpha r} + M \cdot \frac{di_{\alpha s}}{dt} + \omega_r \cdot L_r \cdot i_{\beta r} \\ &\quad + \omega_r \cdot M \cdot i_{\beta s} \\ 0 &= \left(R_r + L_r \cdot \frac{d}{dt}\right) \cdot i_{\beta r} + M \cdot \frac{di_{\beta s}}{dt} - \omega_r \cdot L_r \cdot i_{\alpha r} \\ &\quad - \omega_r \cdot M \cdot i_{\alpha s} \end{aligned} \tag{3}$$

where $L_s = L_{ls} + 3 \cdot L_m$, $L_r = L_{lr} + 3 \cdot L_m$, $M = 3 \cdot L_m$ and ω_r is the rotor electrical speed ($\omega_r = p \cdot \omega$, p being the pole pair number). Subscripts s and r denote stator and rotor variables, respectively. According to the vector space decomposition in distributed-winding machines, the torque production is only limited to the α-β subspace (other subspaces are not involved in the electromechanical energy conversion process and only generate copper losses):

$$T_e = p \cdot M \cdot (i_{\beta r} \cdot i_{\alpha s} - i_{\alpha r} \cdot i_{\beta s}) \tag{4}$$

Considering the VSD model, the post-fault operation needs to maintain the pre-fault torque given by (4), generating the same α-β currents. At the same time, the x-y and 0_+-0_- currents need to be optimized to satisfy the restriction defined in (1).

III. Optimization of Current References for Single and Two Isolated Neutral Points

This section describes the off-line optimization of the post-fault current references for different fault scenarios in single and two neutrals configurations. Opposite to the case with independent dc-links [7-8,26-29], no assumptions are made about the amplitude and phase of any of the stator currents, so they can be written as:

$$\begin{aligned} i_{a1}(t) &= \sqrt{2}\cdot I_{a1}\cdot cos(\omega\cdot t+\varphi_{a1}) \\ i_{b1}(t) &= \sqrt{2}\cdot I_{b1}\cdot cos(\omega\cdot t+\varphi_{b1}) \\ i_{c1}(t) &= \sqrt{2}\cdot I_{c1}\cdot cos(\omega\cdot t+\varphi_{c1}) \\ i_{a2}(t) &= \sqrt{2}\cdot I_{a2}\cdot cos(\omega\cdot t+\varphi_{a2}) \\ i_{b2}(t) &= \sqrt{2}\cdot I_{b2}\cdot cos(\omega\cdot t+\varphi_{b2}) \\ i_{c2}(t) &= \sqrt{2}\cdot I_{c2}\cdot cos(\omega\cdot t+\varphi_{c2}) \end{aligned} \quad (5)$$

Steady-state phase currents in the time domain (5) can be written as phasors in the form $I_{a1}\lfloor\varphi_{a1}$, $I_{a2}\lfloor\varphi_{a2}$, $I_{b1}\lfloor\varphi_{b1}$, $I_{b2}\lfloor\varphi_{b2}$, $I_{c1}\lfloor\varphi_{c1}$ and $I_{c2}\lfloor\varphi_{c2}$. In order to minimize the post-fault drive derating, the objective of the optimization process is to determine the twelve unknowns I_{a1}, I_{b1}, I_{c1}, I_{a2}, I_{b2}, I_{c2}, φ_{a1}, φ_{b1}, φ_{c1}, φ_{a2}, φ_{b2} and φ_{c2} that maximize the electrical torque defined in (4) with minimum torque ripple and some restrictions associated to the fault and winding configuration. It becomes apparent that one should include the model equations (3)-(4) into the optimization process. However, it follows from the machine model that higher α-β current phasor amplitudes produce higher achievable torque. Consequently, it is possible to indirectly find the currents that maximize the torque by maximizing the circular-shaped α-β currents. This procedure simplifies the optimization because no model of the machine is used.

Applying the Clarke transformation to the phase current phasors, one obtains the VSD current phasors $I_\alpha\lfloor\varphi_\alpha$, $I_\beta\lfloor\varphi_\beta$, $I_x\lfloor\varphi_x$, $I_y\lfloor\varphi_y$, $I_{0+}\lfloor\varphi_{0+}$ and $I_{0-}\lfloor\varphi_{0-}$. The circular-shaped rotating phasors are obtained by including the restrictions:

$$\begin{aligned} I_\alpha &= I_\beta \\ \varphi_\alpha &= \varphi_\beta - \pi/2 \end{aligned} \quad (6)$$

Finally, the restrictions associated to the neutral point connection also need to be included. For the two isolated neutrals connection the constraints are:

$$\begin{aligned} i_{a1}(t)+i_{b1}(t)+i_{c1}(t) &= 0 \\ i_{a2}(t)+i_{b2}(t)+i_{c2}(t) &= 0 \end{aligned} \quad (7)$$

while the restriction for the single isolated neutral connection is:

$$i_{a1}(t)+i_{b1}(t)+i_{c1}(t)+i_{a2}(t)+i_{b2}(t)+i_{c2}(t) = 0 \quad (8)$$

Summarizing the cost function and the restrictions of (1), (6) and (7)/(8), the optimization problem can be described as:

$$\max_{(I_{a1},I_{b1},I_{c1},I_{a2},I_{b2},I_{c2},\varphi_{a1},\varphi_{b1},\varphi_{c1},\varphi_{a2},\varphi_{b2},\varphi_{c2})}\{I_\alpha, I_\beta\}$$

Subject to:

- $I_\alpha = I_\beta$
- $\varphi_\alpha = \varphi_\beta - \pi/2$
- $I_\alpha\lfloor\varphi_\alpha = \sqrt{2}\cdot(I_{a1}\lfloor\varphi_{a1} - \frac{1}{2}\cdot I_{b1}\lfloor\varphi_{b1} - \frac{1}{2}\cdot I_{c1}\lfloor\varphi_{c1} + \frac{\sqrt{3}}{2}\cdot I_{a2}\lfloor\varphi_{a2} - \frac{\sqrt{3}}{2}\cdot I_{b2}\lfloor\varphi_{b2})$
- $I_\beta\lfloor\varphi_\beta = \sqrt{2}\cdot(\frac{\sqrt{3}}{2}\cdot I_{b1}\lfloor\varphi_{b1} - \frac{\sqrt{3}}{2}\cdot I_{c1}\lfloor\varphi_{c1} + \frac{1}{2}\cdot I_{a2}\lfloor\varphi_{a2} + \frac{1}{2}\cdot I_{b2}\lfloor\varphi_{b2} - I_{c2}\lfloor\varphi_{c2})$
- $I_k \le \frac{I_n}{2}\ \forall k \in \{\text{Faulted phases}\}$
- $I_k \le I_n\ \forall k \in \{\text{Healthy phases}\}$
- Kirchhoff restrictions (equations (7)or (8))

(9)

that can be solved using the CONOPT optimization method included in the GAMS software [33-35]. CONOPT is based on the Generalized Reduced Gradient technique, being especially reliable on models with differentiable functions. Moreover, this method is suitable for nonlinear problems with few degrees of freedom and a low number of variables, which are the features of the problem defined in (9). However, CONOPT does not guarantee a global optimum solution, so several seeds have been used to avoid local maxima.

In short, the optimization process looks for steady-state phase currents that generate a circular shape of α-β currents with maximum amplitude, satisfying the phase current limits (either I_n or $I_n/2$) and the neutral connection (two or single) restrictions. The circular shape of the α-β currents ensures smooth post-fault operation, the maximum value of α-β currents guarantees minimum drive derating and the restriction on the maximum phase currents ensures operation within the thermal limits of the system.

Solving (9), the unknown variables (twelve in total, corresponding to the amplitudes and phases of the stator phase currents) can be determined from the optimization process for all fault scenarios. Even though there are many possibilities if one considers up to three faults, only some of them are truly independent while the rest correspond to the same solution. For example, a single fault in leg-A_1' is similar to a single fault in leg-B_1' because the remaining healthy and faulty phases have equal spatial shifting. The same applies to the case of two faults in legs A_1'-B_1' and A_1'-C_1'. Carefully examining the spatial displacement of the healthy and faulted phases, it is finally concluded that there are only nine independent fault scenarios:

- Scenario 1: Fault in leg-A_1'.
- Scenario 2: Faults in legs A_1'-B_1'.
- Scenario 3: Faults in legs A_1'-A_2'.
- Scenario 4: Faults in legs A_1'-B_2'.
- Scenario 5: Faults in legs A_1'-C_2'.
- Scenario 6: Faults in legs A_1'-B_1'-C_1'.
- Scenario 7: Faults in legs A_1'-B_1'-C_2'.
- Scenario 8: Faults in legs A_1'-B_1'-A_2'.
- Scenario 9: Faults in legs A_1'-B_1'-B_2'.

The remaining scenarios can be reduced to a spatial shifting of these nine possibilities.

The aforementioned twelve unknowns for scenarios 1 to 5 (one and two faults) and two neutrals connection are shown in Table I. It also includes the maximum achievable α-β current which constitutes an indirect indicator of the maximum achievable torque. It must be noted here that the actual torque depends on the ratio of d-q currents (i_d/i_q) but the maximum modulus of the α-β currents is unique for

TABLE I
OPTIMIZED CURRENT REFERENCES FOR ONE AND TWO OPEN-CIRCUIT FAULTS WITH TWO NEUTRALS

Fault Scenario	**1 (a_1)**	**2 (a_1-b_1)**	**3 (a_1-a_2)**	**4 (a_1-b_2)**	**5 (a_1-c_2)**
I_{a1} (p.u.)	0.5	0.5	0.5	0.5	0.5
I_{b1} (p.u.)	1	0.5	0.71	1	1
I_{c1} (p.u.)	1	0.5	1	0.71	1
I_{a2} (p.u.)	1	1	0.5	1	1
I_{b2} (p.u.)	1	1	1	0.5	1
I_{c2} (p.u.)	0.5	1	0.71	0.71	0.5
φ_{a1} (°)	10.43	4.64	13.07	12.04	10.43
φ_{b1} (°)	114.91	124.64	82.30	150.68	114.91
φ_{c1} (°)	265.95	244.64	234.43	302.81	265.95
φ_{a2} (°)	24.91	34.64	32.00	34.47	24.91
φ_{b2} (°)	175.95	154.64	170.65	173.11	175.95
φ_{c2} (°)	280.43	274.64	322.77	242.34	280.43
$\lvert I_{\alpha\beta}\rvert$ (A)	1.98	1.84	1.61	1.61	1.98
$\lvert I_{\alpha\beta}\rvert$ (p.u.)	0.81	0.75	0.66	0.66	0.81
i_x^*	$-0.38\cdot i_\alpha^*$	$-0.33\cdot i_\alpha^*$	$-0.24\cdot i_\alpha^* + 0.07\cdot i_\beta^*$	$-0.24\cdot i_\alpha^* - 0.07\cdot i_\beta^*$	$-0.38\cdot i_\alpha^*$
i_y^*	$-0.38\cdot i_\beta^*$	$0.33\cdot i_\beta^*$	$-0.76\cdot i_\alpha^* - 0.24\cdot i_\beta^*$	$0.76\cdot i_\alpha^* - 0.24\cdot i_\beta^*$	$-0.38\cdot i_\beta^*$

TABLE II
OPTIMIZED CURRENT REFERENCES FOR ONE AND TWO OPEN-CIRCUIT FAULTS WITH SINGLE NEUTRAL

Fault Scenario	**1 (a_1)**	**2 (a_1-b_1)**	**3 (a_1-a_2)**	**4 (a_1-b_2)**	**5 (a_1-c_2)**
I_{a1} (p.u.)	0.5	0.5	0.5	0.5	0.5
I_{b1} (p.u.)	1	0.5	1	1	1
I_{c1} (p.u.)	1	1	1	1	1
I_{a2} (p.u.)	1	1	0.5	1	1
I_{b2} (p.u.)	1	1	1	0.5	1
I_{c2} (p.u.)	1	1	1	1	0.5
φ_{a1} (°)	11.79	0	16.46	10.91	10.43
φ_{b1} (°)	103.38	127.64	80.40	136.09	114.91
φ_{c1} (°)	226.26	223.37	213.35	222.10	265.95
φ_{a2} (°)	19.24	32.76	19.76	30.10	24.91
φ_{b2} (°)	168.39	140.50	182.88	155.28	175.95
φ_{c2} (°)	297.96	297.58	315.83	304.09	280.43
$\lvert I_{\alpha\beta}\rvert$ (A)	2.14	1.97	1.71	1.95	1.98
$\lvert I_{\alpha\beta}\rvert$ (p.u.)	0.87	0.81	0.70	0.80	0.81
i_x^*	$-0.27\cdot i_\alpha^* - 0.04\cdot i_\beta^*$	$-0.15\cdot i_\alpha^* + 0.10\cdot i_\beta^*$	$-0.23\cdot i_\alpha^* - 0.12\cdot i_\beta^*$	$0.02\cdot i_\alpha^* - 0.08\cdot i_\beta^*$	$-0.38\cdot i_\alpha^*$
i_y^*	$-0.34\cdot i_\alpha^* - 0.11\cdot i_\beta^*$	$-0.32\cdot i_\alpha^* + 0.23\cdot i_\beta^*$	$-0.90\cdot i_\alpha^* - 0.23\cdot i_\beta^*$	$-0.16\cdot i_\alpha^* + 0.02\cdot i_\beta^*$	$-0.38\cdot i_\beta^*$
i_{0+}^*	$-0.16\cdot i_\alpha^* + 0.14\cdot i_\beta^*$	$-0.22\cdot i_\alpha^* - 0.11\cdot i_\beta^*$	$-0.07\cdot i_\alpha^* + 0.28\cdot i_\beta^*$	$-0.40\cdot i_\alpha^* + 0.11\cdot i_\beta^*$	0
i_{0-}^*	$0.16\cdot i_\alpha^* - 0.14\cdot i_\beta^*$	$0.22\cdot i_\alpha^* + 0.11\cdot i_\beta^*$	$0.07\cdot i_\alpha^* - 0.28\cdot i_\beta^*$	$0.40\cdot i_\alpha^* - 0.11\cdot i_\beta^*$	0

TABLE III
OPTIMIZED CURRENTS FOR THREE OPEN-CIRCUIT FAULTS WITH TWO NEUTRALS

Fault Scenario	**6 ($a_1-b_1-c_1$)**	**7 ($a_1-b_1-c_2$)**	**8 ($a_1-b_1-a_2$)**	**9 ($a_1-b_1-b_2$)**
I_{a1} (p.u.)	0.5	0.5	0.5	0.5
I_{b1} (p.u.)	0.5	0.5	0.5	0.5
I_{c1} (p.u.)	0.5	0.872	0.872	0.5
I_{a2} (p.u.)	1	0.794	0.5	0.5
I_{b2} (p.u.)	1	1	1	0.5
I_{c2} (p.u.)	1	0.5	0.794	0.5
φ_{a1} (°)	4.64	58.06	24.72	9.9
φ_{b1} (°)	124.64	116.71	83.37	129.9
φ_{c1} (°)	244.64	267.38	234.05	249.9
φ_{a2} (°)	34.64	5.08	37.76	39.9
φ_{b2} (°)	154.64	155.45	165.99	159.9
φ_{c2} (°)	274.64	283.68	316.36	279.9
$\lvert I_{\alpha\beta}\rvert$ (A)	1.84	1.55	1.55	1.23
$\lvert I_{\alpha\beta}\rvert$ (p.u.)	0.75	0.63	0.63	0.5
i_x^*	$-0.33\cdot i_\alpha^*$	$-0.47\cdot i_\alpha^* + 0.59\cdot i_\beta^*$	$-0.23\cdot i_\alpha^* + 0.18\cdot i_\beta^*$	0
i_y^*	$0.33\cdot i_\beta^*$	$-0.05\cdot i_\alpha^* - 0.21\cdot i_\beta^*$	$-0.72\cdot i_\alpha^* + 0.03\cdot i_\beta^*$	0

TABLE IV
OPTIMIZED CURRENT AMPLITUDES FOR THREE OPEN-CIRCUIT FAULTS WITH SINGLE NEUTRAL

Fault Scenario	**6 ($a_1-b_1-c_1$)**	**7 ($a_1-b_1-c_2$)**	**8 ($a_1-b_1-a_2$)**	**9 ($a_1-b_1-b_2$)**
I_{a1} (p.u.)	0.5	0.5	0.5	0.5
I_{b1} (p.u.)	0.5	0.5	0.5	0.5
I_{c1} (p.u.)	0.5	1	1	1
I_{a2} (p.u.)	1	1	0.5	1
I_{b2} (p.u.)	1	1	1	0.5
I_{c2} (p.u.)	1	0.5	1	1
φ_{a1} (°)	4.64	9.55	36.52	0
φ_{b1} (°)	124.64	154.28	87.54	180.40
φ_{c1} (°)	244.64	275.23	229.40	243.75
φ_{a2} (°)	34.64	59.04	41.45	93.09
φ_{b2} (°)	154.64	167.55	169.68	181.05
φ_{c2} (°)	274.64	311.04	326.77	354.89
$\lvert I_{\alpha\beta}\rvert$ (A)	1.84	1.81	1.61	1.55
$\lvert I_{\alpha\beta}\rvert$ (p.u.)	0.75	0.74	0.66	0.63
i_x^*	$-0.33\cdot i_\alpha^*$	$-0.26\cdot i_\alpha^* + 0.10\cdot i_\beta^*$	$-0.18\cdot i_\alpha^* + 0.21\cdot i_\beta^*$	$0.07\cdot i_\alpha^* - 0.38\cdot i_\beta^*$
i_y^*	$0.33\cdot i_\beta^*$	$-0.07\cdot i_\alpha^* - 0.04\cdot i_\beta^*$	$-0.88\cdot i_\alpha^* + 0.11\cdot i_\beta^*$	$-0.53\cdot i_\alpha^* + 0.38\cdot i_\beta^*$
i_{0+}^*	0	$-0.09\cdot i_\alpha^* - 0.31\cdot i_\beta^*$	$-0.11\cdot i_\alpha^* + 0.05\cdot i_\beta^*$	$-0.50\cdot i_\alpha^* - 0.18\cdot i_\beta^*$
i_{0-}^*	0	$0.09\cdot i_\alpha^* + 0.31\cdot i_\beta^*$	$0.11\cdot i_\alpha^* - 0.05\cdot i_\beta^*$	$0.50\cdot i_\alpha^* + 0.18\cdot i_\beta^*$

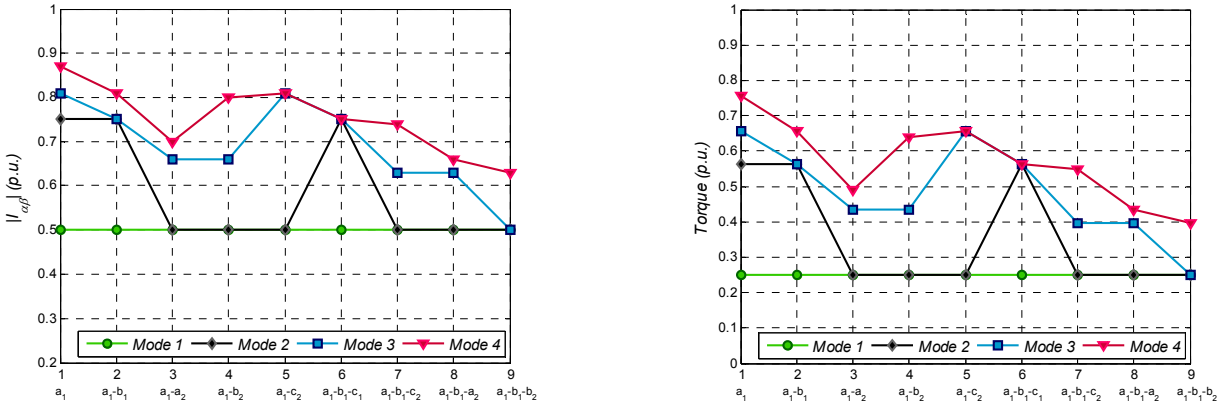

Fig. 2. Maximum amplitude of the α-β current phasor and torque for different fault scenarios in modes 1 (green), 2 (black), 3 (blue) and 4 (red).

each fault. For this reason this study focuses on the achievable current rather than the achievable torque, which is different for each flux setting. Table II replicates the same results of scenarios 1 to 5 but for single neutral connection, showing that the additional degree of freedom results in higher achievable post-fault modulus of the *α-β* currents. Table III and IV present the scenarios 6 to 9 (three faults) for two neutrals and single neutral connection, respectively.

Even though the optimized values of unknowns included in Tables I to IV provide the desired steady-state performance, the field oriented control (FOC) of the multiphase induction motor drive requires instantaneous current references both in steady-state and transient conditions. A further step is required to find the *x-y* and 0_+-0_- current references to obtain high performance post-fault operation. The currents in the secondary planes are related to the optimized values of *α-β* currents, and this relationship is used to obtain instantaneous references for the FOC stage. As an example, the scenario 1 with single fault in leg-A_1' implies for two neutrals connection:

$$\begin{aligned} i_x^* &= -0.38 \cdot i_\alpha^* \\ i_{0+}^* &= i_{0-}^* = 0 \\ i_y^* &= -0.38 \cdot i_\beta^* \end{aligned} \tag{10}$$

while for single neutral connection one obtains:

$$\begin{aligned} i_x^* &= -0.27 \cdot i_\alpha^* - 0.04 \cdot i_\beta^* \\ i_{0+}^* &= -0.16 \cdot i_\alpha^* + 0.14 \cdot i_\beta^* \\ i_y^* &= -0.34 \cdot i_\alpha^* - 0.11 \cdot i_\beta^* \\ i_{0-}^* &= 0.16 \cdot i_\alpha^* - 0.14 \cdot i_\beta^* \end{aligned} \tag{11}$$

Tables I and III include the relationship between *x-y* and *α-β* currents for scenarios 1 to 9 and two neutrals (grey background) that will be used for control purposes (section IV). In the case of single neutral connection (Tables II and IV), the zero sequence can flow ($i_{0+} = -i_{0-} \neq 0$) and the tables include the relationship for both *x-y* and 0_+-0_- currents (grey background).

To sum up, the optimization process of (9) has provided the amplitude and phase of stator currents for scenarios 1 to 9 in single and two neutrals configurations, and the relationship between *x-y* and 0_+-0_- currents with *α-β* currents settles the basis for the control references to properly track the optimum phase currents.

For the sake of visualization and easy understanding, the maximum achievable amplitude of the *α-β* current is depicted in Fig. 2, considering four modes of operation:

- Mode 1: Balanced drive operation using pre-fault control and null *x-y* references (e.g. a fault in leg-A_1' reduces the currents in all phases to $I_n/2$), shown in green trace.
- Mode 2: Balanced operation of the faulted VSC (e.g. a fault in leg-A_1' only reduces the currents of phases a_1, b_1 and c_1 to $I_n/2$ [26-27]), shown in black trace.
- Mode 3: Optimized operation with two neutrals (tables I and III), shown in blue trace.
- Mode 4: Optimized operation with single neutral (tables II and IV), shown in red trace.

For the scenario 1 of single fault in leg-A_1' the maximum achievable amplitude of the *α-β* currents is 50%, 75%, 81% and 87% for modes 1 to 4, respectively (Fig. 2, upper plot). Assuming that the *d-q* currents are proportionally reduced, the achievable power is proportional to the square of the current, providing a maximum achievable post-fault torque of 25%, 56%, 65% and 76% for modes 1 to 4, respectively (Fig. 2, lower plot). The gain of modes 3-4 in terms of post-fault torque capability is significant compared to modes 1-2 with symmetrical current supply, being 303% higher in mode 4 compared to mode 1. The scenario 5 with faults in legs A_1' and C_2' provides maximum achievable amplitude of 50% and 81% of the nominal one for the *α-β* currents and modes 1-2 and 3-4, respectively, resulting in post-fault torques of 25% and 65% of the nominal one. The post-fault achievable torque is now 260% higher in the optimized cases (3-4) compared to the cases with balanced operation (1-2). In general, the *d-q* currents may not be reduced proportionally and the gain in terms of post-fault achievable torque would be different, but in any case the derating of the drive is highly alleviated with the optimized currents detailed in Tables I to IV.

Nevertheless, the previously optimized current references need to be tracked by proper control strategies that may need to be modified after the fault occurrence, as it is described next.

IV. Post-fault Control Scheme

The general structure of the pre-fault control strategy is shown in Fig. 3. The scheme is an indirect rotor field oriented control (IRFOC) with an outer speed control loop and inner current control loops for *d-q*, *x-y*, and 0_+-0_- currents. Four/five phase currents need to be measured in the two/single neutral configurations because the remaining phase currents can be obtained from the condition of having two/one isolated neutral points. Measured phase currents are converted into *α-β* currents using the Clarke transformation $[T_6]$ of (2) and *d-q* currents are obtained from the rotation of *α-β* currents in the forward (synchronous) direction using the Park transformation:

$$[D] = \begin{bmatrix} cos\theta_s & sin\theta_s \\ -sin\theta_s & cos\theta_s \end{bmatrix} \tag{12}$$

where the angle θ_s of the rotating reference frame is obtained from the measured speed ω and the estimated slip:

$$\theta_s = \int \left(p \cdot \omega - \frac{i_q^*}{T_r i_d^*} \right) dt \tag{13}$$

being T_r the rotor time constant.

The machine is fluxed setting a value of i_d^* that corresponds with the rated flux of the machine and the torque is regulated by the outer speed control loop that provides the reference of the quadrature current i_{qs}^*. The output of the *d-q* current controllers and the decoupling terms e_d and e_q [1], provide the reference voltages v_d^* and v_q^*. The other inner current loops correspond to the *x-y* and 0_+-0_- current control, which can be performed in stationary frame using the Clarke transformation $[T_6]$, in synchronous frame using the Park transformation $[D]$ or in anti-

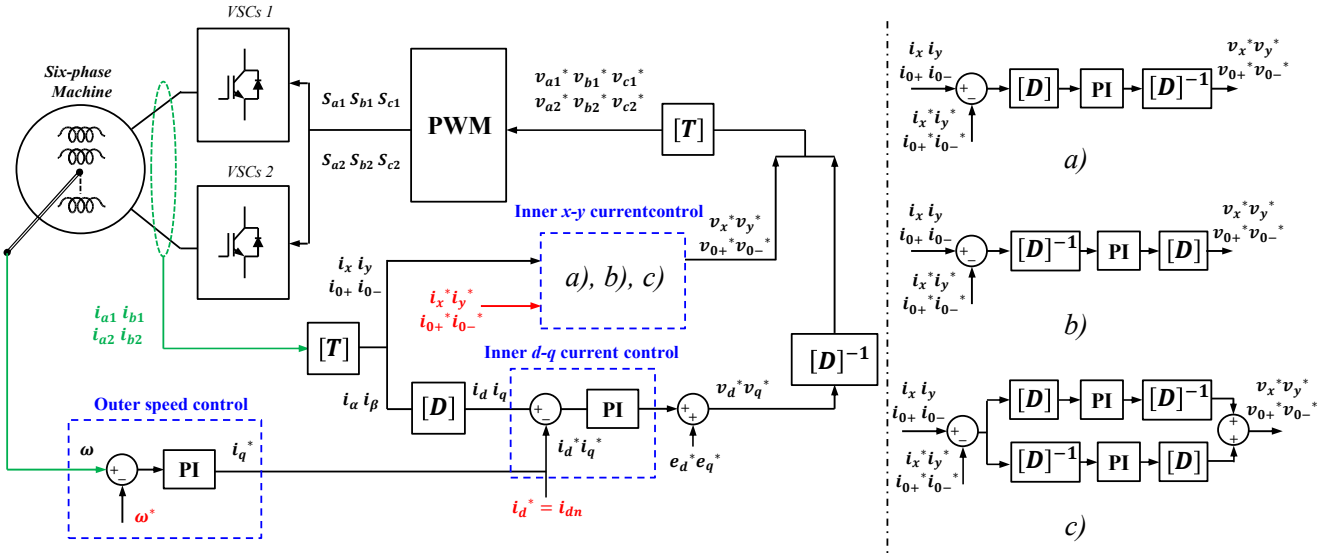

Fig. 3. Field oriented control (FOC) of the six-phase induction machine with synchronous *d-q* current control and different *x-y* controllers: a) Synchronous, b) Anti-synchronous and c) Resonant (dual PI).

synchronous frame using the inverse of the Park transformation $[D]^{-1}$:

$$[D]^{-1} = \begin{bmatrix} cos\theta_s & -sin\theta_s \\ sin\theta_s & cos\theta_s \end{bmatrix} \quad (14)$$

In two neutrals configurations the zero sequence components are null, and consequently there is no need to include currents controllers for 0_+-0_- current components. On the contrary, the single neutral configuration allows the flow zero sequence currents and an additional controller for 0_+-0_- current components is required (Fig. 3). In pre-fault situation, both *x-y* and 0_+-0_- current references are set to zero and PI controllers suffice to adequately track these null values.

Now, in post-fault situation the asymmetric phase current references obtained from the optimization process result in non-zero *x-y*, and 0_+-0_- currents. If these components of the secondary planes can be rotated in such a way that they are constant, it will be possible to still maintain PI controllers. Otherwise, the bandwidth of PI controllers will be insufficient to adequately track the variable references and resonant controllers (PR) will be required [36-37]. For example, the scenario when leg-A_1' is faulted in two neutrals configuration (first column in table I), the *x-y* components are inversely proportional to *α-β* and a rotation in the forward (synchronous) direction using Park transformation (12) provides constant *x-y* references. In such a case it is possible to use the synchronous controllers of Fig. 3a together with single PI controllers. In the cases when legs A_1' and B_1' are faulted in two neutrals configuration (Table I, second column) or when legs A_1', B_1' and C_1' are faulted either in single or two neutral configuration (Tables III and IV), the *x*-current is inversely proportional to the *α*-current while the *y*-current is directly proportional to the *β*-current. In this case the only way to obtain constant *x-y* references is to perform a rotation in backwards direction (anti-synchronous) using the inverse Park transformation of (14). Single PI controllers are still applicable in these cases (Fig. 3b). In all other cases, the *x-y* and 0_+-0_- current references depend on the *α-β* references in a way that there is no reference frame where the components of the secondary plane remain constant. In these cases single PI controllers become insufficient and it is necessary to implement resonant controllers in the form of dual-PI controllers in both synchronous and anti-synchronous directions (Fig. 3c) [37]. The dual-PI controllers can adequately track both positive and negative current components and thus follow non-constant *x-y*, and 0_+-0_- current references.

To sum up, the post-fault control strategy maintains the same pre-fault FOC scheme and the only changes that need to be performed are:

1) Modify the *x-y* and 0_+-0_- current references according to the type of fault (Table I to IV).
2) Modify the *x-y* and 0_+-0_- current controllers to synchronous PI, anti-synchronous PI or dual PI controllers.

Finally, the output of the *x-y* and 0_+-0_- current controllers provides the *x-y* and 0_+-0_- voltage references. The *d-q*, *x-y* and 0_+-0_- reference voltages are then anti-transformed using the Park ($[D]$ and $[D]^{-1}$) and Clarke ($[T_6]$) matrices to provide the phase voltage references ($v_{a1}^* v_{b1}^* v_{c1}^* v_{a2}^* v_{b2}^* v_{c2}^*$) that are inputs for the carrier-based six-phase PWM, generating finally the switching signals to VSCs1 and VSCs2.

V. Experimental Results

This section describes the test bench and presents the experimental results of the post-fault operation, resulting from the previously described current reference calculation (section III) and control strategy (section IV).

A. Test Bench

A three-phase induction machine (IM) has been rewound to obtain the asymmetrical six-phase induction machine (IM) shown in the scheme of Fig. 3. Parameters of the custom-built six-phase machine have been determined using AC-time domain and stand-still with inverter supply tests [38-39], providing stator and rotor resistances of 4.2 and 2 Ω, stator and rotor leakage inductances of 4.2 and 55 mH, and mutual inductance of 420 mH. Table V presents the rated values of the tested motor. This six-phase machine is driven by two conventional three-phase power converters from Semikron (SKS22F modules) that correspond to VSCs1 and VSCs2 in Fig. 1. The converters are connected to a DC power supply system as in Fig. 1a, and the control actions are performed by a digital signal processor (TMS320F28335 from Texas Instruments, TI). The control unit is programmed using a JTAG and the TI proprietary software called Code Composer Studio. Current and speed measurements are taken with four hall-effect sensors (LEM LAH 25-NP) and a digital encoder (GHM510296R/2500), respectively. The load torque is provided by a DC-machine whose armature is connected to a variable resistive-inductive load. The full scheme of the test bench is described in Fig. 4. Tables VI and VII show the gain of the controllers employed in the tests. These controllers have been adjusted to obtain similar outcomes of overshooting and rising time in pre and post-fault situations.

B. Experimental Results

The experimental tests that follow are performed setting a flux reference i_d^* = 1A, a rated q-current of 8A, a switching frequency of 10 kHz and a dc-link voltage of V_{dc} = 300V. Although the fault detection delay using PR controllers affects the transient to some extent [36], this work focuses on the optimized steady-state post-fault performance, and the delay is not considered in the experiments. A subset of the nine scenarios considered in section III are experimentally tested to verify the smooth performance of the drive and the current tracking capability of the suggested control scheme.

The scenario 1 with a fault in leg-A_1' and two neutrals configurations is examined first. The machine is operated in healthy mode until t = 10 s with zero x-y currents, d-current controlled to its rated value of 1A, and a constant q-current to provide the necessary torque to drive the machine at 500 rpm (Fig. 5). After the fault occurrence at t = 10 s the x-y references are changed to the values calculated in Table I and the control scheme uses the synchronous controllers shown in Fig. 3a. The transition from pre- to post-fault states is smooth with no appreciable impact on the d-q currents (Fig. 5b) or motor speed (Fig. 5a). The x-y currents prove to track the non-null post-fault references providing a fast adaptation to the new situation (Fig. 5c). The modification of the x-y currents provokes the desired imbalance in the phase currents, increasing the amplitude of phases b_1, c_1, a_2 and b_2, and decreasing the amplitude of phases a_1 and c_2 (Fig. 5d and 5e). Phase shifting between phase currents is also modified in accordance to the values

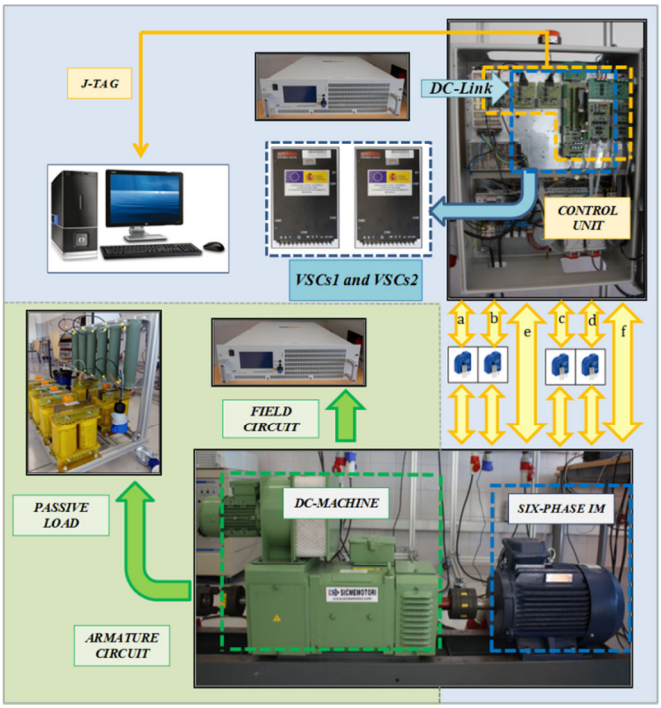

Fig. 4: Scheme of the test bench used for the experimental results.

TABLE V
RATED VALUES OF THE MOTOR

Power (kW)	0.9
I_{peak}(A)	4.7
i_d(A)	1.0
i_q(A)	8.0
ω_r(rpm)	1000.0

TABLE VI
VALUES OF SYNCHRONOUS AND ANTI-SYNCHRONOUS CONTROLLERS

Controller	K_P	K_I
PI ω	0.50	3.50
PI d current	100.00	150.00
PI q current	50.00	20.00
PI x current	20.00	10.00
PI y current	20.00	10.00
PI 0_+ current	0.01	1.00
PI 0_- current	0.01	1.00

TABLE VII
VALUES OF DUAL PI CONTROLLERS

Controller	K_P	K_I
PI ω	0.50	3.50
PI d current	100.00	150.00
PI q current	50.00	20.00
PI x current	12.50	322.00
PI y current	12.50	322.00
PI 0_+ current	0.01	1.00
PI 0_- current	0.01	1.00

predicted in table I. The theoretical optimal phase currents from GAMS are shown in Fig. 5d and 5e with black traces, showing a good agreement between theoretical and experimental values. The three most significant conclusions from the test are: *i*) the transition from pre- to post operation is performed smoothly, *ii*) the synchronous control of x-y currents with simple PI controllers is

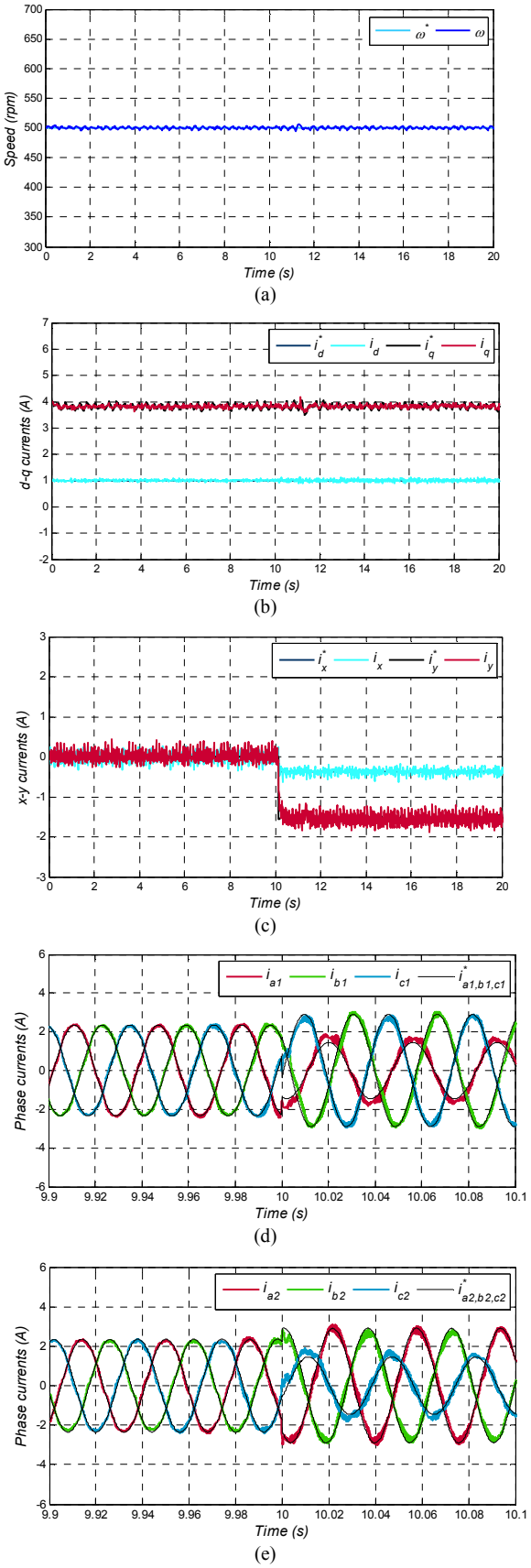

Fig. 5. Transition from pre- to post-fault operation when leg-A_1' is faulted in two neutrals configuration: a) Motor speed, b) d-q currents, c) x'-y' currents, d) phase currents in $a_1b_1c_1$ and e) phase currents in $a_2b_2c_2$.

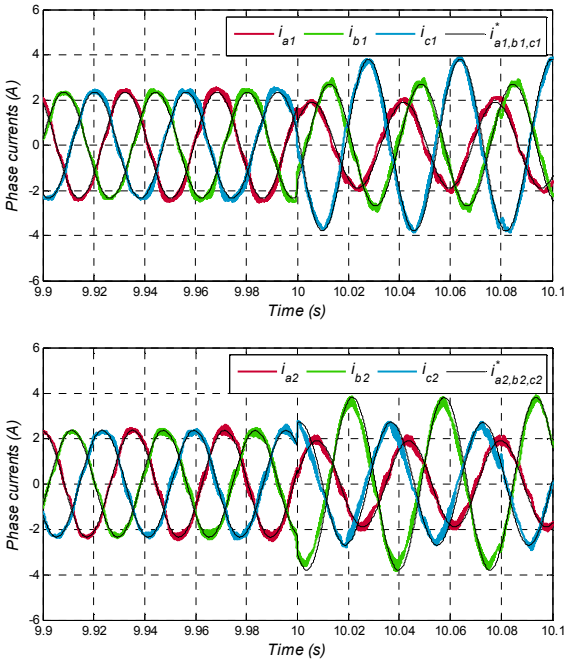

Fig. 6. Transition from pre- to post-fault operation when legs A_1' and A_2' are faulted in two neutrals configuration. Phase currents in $a_1b_1c_1$ (upper plot) and $a_2b_2c_2$ (lower plot).

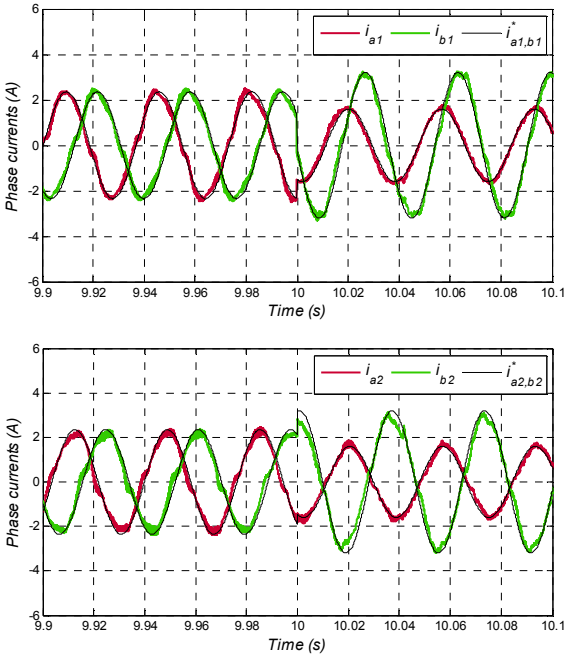

Fig. 7. Transition from pre- to post-fault operation when legs A_1' and A_2' are faulted in single neutral configuration. Phase currents in a_1b_1 (upper plot) and a_2b_2 (lower plot).

sufficient to track the non-null post-fault references and *iii*) the modification of the x-y current references provokes an imbalance that maintains the drive within post-fault rated values (1). As far as the motor speed and d-q currents are concerned, their waveforms in other fault scenarios are essentially similar to those shown in Fig. 5a and 5b, so only phase currents will be shown next. Fig. 6 shows phase currents for scenario 3, when legs A_1' and A_2' are faulted in

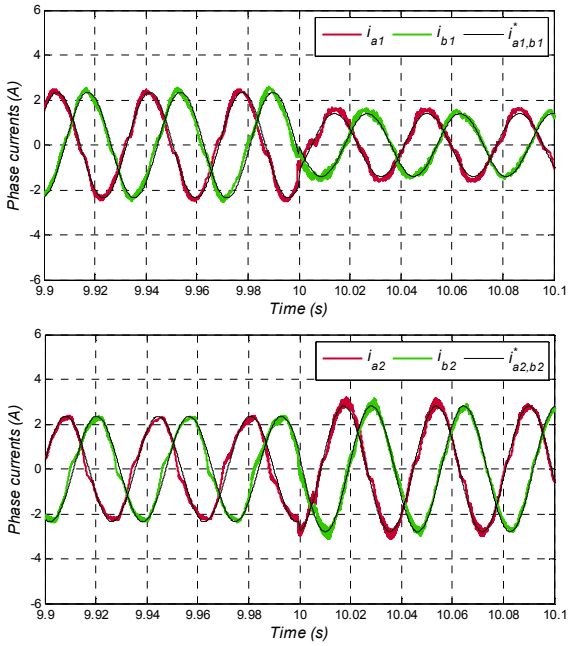

Fig. 8. Transition from pre- to post-fault operation when legs A_1' and B_1' are faulted in two neutrals configuration: a) phase currents in a_1b_1 and b) phase currents in a_2b_2.

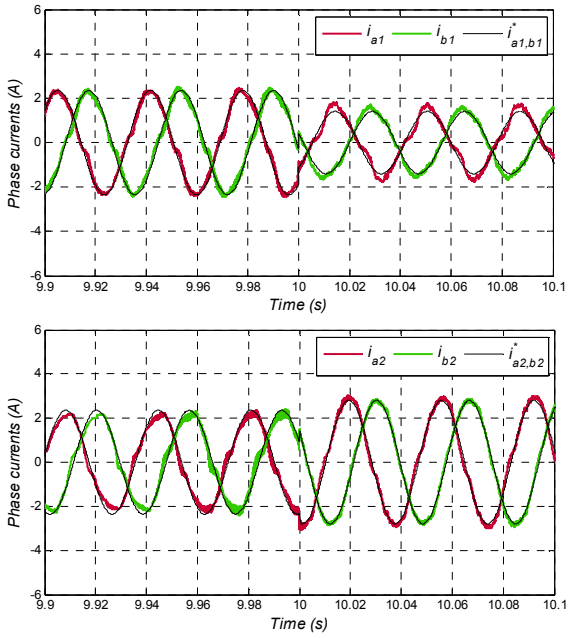

Fig. 9. Transition from pre- to post-fault operation when legs A_1', B_1' and C_2' are faulted in single neutral configuration. Phase currents in a_1b_1 (upper plot) and a_2b_2 (lower plot).

two neutrals configuration (Table I). As predicted, three different amplitudes of phase currents are obtained in each of the two sets of three-phase windings. Since both x and y current references do not only depend on α and β, respectively, there is no reference frame where the x-y currents can be rotated to obtain constant values. For this reason the control is performed using the dual-PI (resonant) controllers shown in Fig. 3c. Optimal current references from GAMS are again shown using black traces. It can be observed that the measured currents satisfactorily match

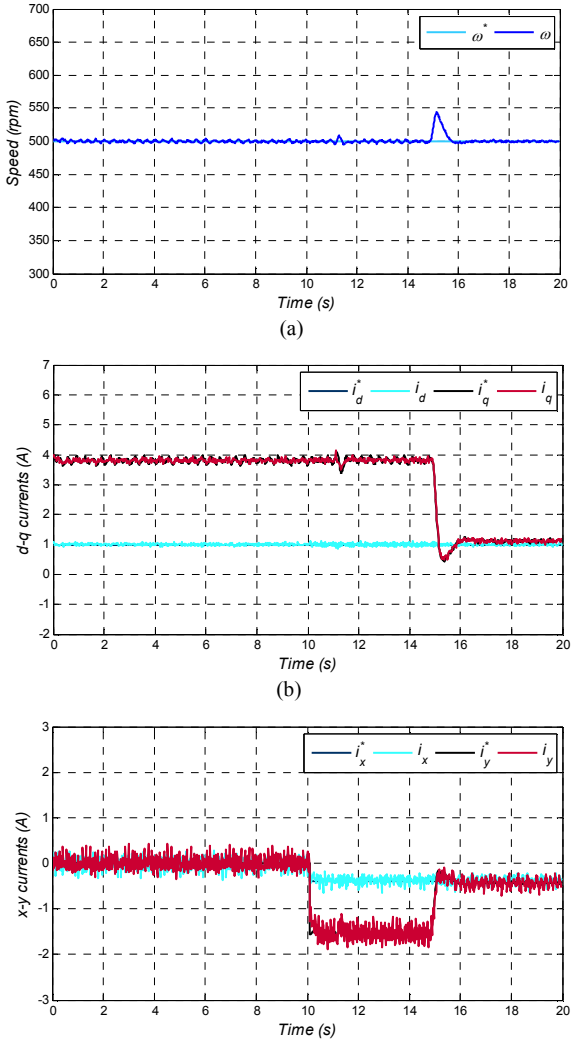

Fig. 10. Dynamic test. Experimental results in the unload test transition at 500 rpm. From top to bottom: motor speed, d-q currents and x-y currents.

their reference values. The currents in phases a_1 and a_2 are adequately reduced to comply with restrictions of (1) and consequently, the drive operates within the permissible limits.

The same fault scenario 3 is tested again but with single neutral connection (Fig. 7). The control of x-y currents is also performed using the dual-PI (resonant) controllers of Fig. 3c but in this case it is also necessary to activate the 0_+-0_- current control because the single neutral connection allows the flow of zero sequence currents from both sets of three-phase windings. Only four currents could be measured so Fig. 7 shows phase currents in a_1-a_2 (faulted phases) and b_1-b_2 (healthy phases). Optimal currents (black traces) are again tracked in post-fault situation, reducing the current in faulted phases to comply with (1).

The next experimental test deals with scenario 2 for single neutral connection (Fig. 8). The relationship of x-y and 0_+-0_- currents with α-β currents (Table II) is such that dual-PI controllers are again required for proper current control. It can be observed that the currents a_2-b_2 are increased while currents a_1-b_1 are decreased in order to

maintain the same pre-fault α-β currents and simultaneously comply with the fault restrictions. The resonant controllers are known to need some cycles to fully adapt to the new references, but the current tracking is again satisfactory.

A final steady-state test considering fault scenario 7 with single neutral connection (table IV) is presented in Fig. 9. The results with three faults are essentially similar to the previous ones involving one and two faults. The response of the current tracking after the fault occurs is fast and the new steady state post-fault currents are adequately tracked.

Experimental results from Figs. 5-9 confirm that: *i*) the *x*-*y* and 0_+-0_- current references derived in Tables I to IV can correctly provide unbalanced phase currents to comply with the fault restrictions and *ii*) the control scheme of Fig. 3 can adequately track the post-fault non-null *x*-*y* and 0_+-0_- current references. As in the case of open-phase faults [29], the non-null currents in the secondary planes results in higher copper losses but it is highly compensated by the increase in the achievable torque.

It must be highlighted that the relationship of *x*-*y* and 0_+-0_- currents included at the bottom of tables I to IV is generally valid for all operating points if the goal is to maximize the post-fault achievable torque. Consequently, the current waveforms for other operating points would be similar (scaled) to those shown in Figs. 5-9 if the fault scenario is the same.

Since the post-fault control only modifies the non-torque-related *x*-*y* and 0_+-0_- currents, the post-fault transient performance is expected to be similar as in healthy condition. Fig. 10 shows the transient performance of the drive under scenario 1 with two neutrals. After t = 10 s the drive operates in post-fault mode and in t = 15 s the machine is disconnected from the dc-machine and it is suddenly unloaded. The speed is transiently increased (Fig. 10a) but the *q*-current is decreased (Fig.10b) to bring the motor back to the reference speed. Since the *y*-current is proportional to the *q*-current, the sudden unload also affects its reference value, which is decreased in no-load operation (Fig. 10c). On the contrary, α- and *x*- currents references are not affected by the transient, showing a good decoupling from *q*- and *y*- currents. The main conclusion is that a satisfactory post-fault dynamic performance is obtained, this being extendable to the other faulty scenarios.

VI. Conclusions

The need for multiple three-phase converters in high-power low-voltage energy conversion systems allows different arrangements and topologies. This work analyzes the fault-tolerant capability of six-phase machines supplied by parallel converters. It is found that optimal unbalanced currents can considerably improve the torque/power capability of the drive compared to other modes of operation with balanced stator/converter currents. Single neutral connection results in higher post-fault torque/power at the expense of a more complex control compared to the case with two isolated neutrals. Optimal currents references can be obtained if proper secondary plane *x*-*y* currents and control strategies are adopted. Although some fault scenarios allow maintaining the pre-fault PI control, the majority of cases require the use of resonant controllers in order to track non-constant references. Experimental results show that appropriate post-fault current references and control strategies result in optimal currents that reduce the drive derating and enhance post-fault performance.

References

[1] E. Levi, R. Bojoi, F. Profumo, H.A. Toliyat and S. Williamson, "Multiphase induction motor drives - A technology status review," *IET Electric Power Applications*, vol. 1, no. 4, pp. 489-516, 2007.

[2] E. Levi, "Multiphase electric machines for variable-speed applications," *IEEE Trans. Ind. Electron.*, vol. 55, no. 5, pp. 1893-1909, 2008.

[3] X. Huang, A. Googman, C. Gerada, Y. Fang and Q. Lu, "Design of a five-phase brushless DC motor for a safety critical aerospace application," *IEEE Trans. Ind. Electron.*, vol. 59, no. 9, pp. 3532-3541, 2012.

[4] W. Cao, B.C. Mecrow, G.J. Atkinson, J.W. Bennett and D.J. Atkinson, "Overview of electric motor technologies used for more electric aircraft (MEA)" *IEEE Trans. Ind. Electron.*, vol. 59, no. 9, pp. 3523-3531, 2012.

[5] M. Liserre, R. Cárdenas, M. Molinas, and J. Rodríguez, "Overview of multi-MW wind turbines and wind parks," *IEEE Trans. Ind. Electron.*, vol. 58, no. 4, pp. 1081–1095, 2011.

[6] B. Wu, Y. Lang, N. Zargari, and S. Kouro, "*Power conversion and control of wind energy systems*," IEEE Press - John Wiley and Sons, Hoboken, NJ, 2011.

[7] E. Jung, H. Yoo, S. Sul, H. Choi and Y. Choi, "A nine-phase permanent-magnet motor drive system for an ultrahigh-speed elevator," *IEEE Trans. Ind. Appl.*, vol. 48, no. 3, pp. 987-995, 2012.

[8] "Gamesa 5.0 MW" Gamesa Technological Corporation S.A., 2014. Online available: http://www.gamesacorp.com/recursos/doc/productos-servicios/aerogeneradores/catalogo-g10x-45mw.pdf

[9] L. Zarri, M. Mengoni, Y. Gritli, A. Tani, F. Filippetti, G. Serra and D. Casadei, "Detection and localization of stator resistance dissymmetry based on multiple reference frame controllers in multiphase induction motor drives," *IEEE Trans. Ind. Electron.*, vol. 60, no. 8, pp. 3506-3518, 2013.

[10] M. Salehifar, R.S. Arashloo, J.M. Moreno-Equilaz, V. Sala and L. Romeral, "Fault detection and fault tolerant operation of a five phase PM motor drive using adaptive model identification approach," *IEEE Trans. Emerg. Sel. Topics Power Electron.*, vol. 2, no. 2, pp. 212-223, 2014.

[11] X. Kestelyn and E. Semail, "A vectorial approach for generation of optimal current references for multiphase permanent-magnet synchronous machines in real time," *IEEE Trans. Ind. Electron.*, vol. 58, no. 11, pp. 5057-5065, 2011.

[12] N. Bianchi, S. Bolognani and M.D. Pré, "Strategies for the fault-tolerant current control of a five-phase permanent-magnet motor," *IEEE Trans. Ind. Appl.*, vol. 43, no. 4, pp. 960-970, 2007.

[13] A.S. Abdel-Khalik, M.I. Masoud, S. Ahmed and A. Massoud, "Calculation of derating factors based on steady-state unbalanced multiphase induction machine model under open phase(s) and optimal winding currents," *Electric Power System Research*, vol. 106, pp. 214-225, 2014.

[14] H. Guzmán, M.J. Duran, F. Barrero, B. Bogado and S. Toral, "Speed control of five-phase induction motors with integrated open-phase fault operation using model-based predictive current control techniques," *IEEE Trans. Ind. Electron.*, vol. 61, no. 9, pp. 4474-4484, 2014.

[15] H. Guzmán, F. Barrero and M.J. Duran, "IGBT-gating failure effect on a fault-tolerant predictive current controlled 5-phase induction motor drive," *IEEE Trans. Ind. Electron.*, vol. 62, no. 1, pp. 15-20, 2015.

[16] A. Tani, M. Mengoni, L. Zarri, G. Serra and D. Casadei, "Control of multiphase induction motors with an odd number of phases under open-circuit phase faults," *IEEE Trans. Power Electron.*, vol. 27, no. 2, pp. 565-577, 2012.

[17] A. Mohammadpour, S. Sadeghi and L. Parsa, "A generalized fault-tolerant control strategy for five-phase PM motor drives considering star, pentagon, and pentacle connections of stator windings," *IEEE Trans. Ind. Electron.*, vol. 61, no. 1, pp. 63-75, 2014

[18] A. Mohammadpour and L. Parsa, "A unified fault-tolerant current control approach for five-phase PM motors with trapezoidal back EMF under different stator winding connections," *IEEE Trans. Power Electron.*, vol. 28, no. 7, pp. 3517-3527, 2013.

[19] F. Betin and G.A. Capolino, "Shaft positioning for six-phase induction machines with open phases using variable structure control," *IEEE Trans. Ind. Electron.*, vol. 59, no. 6, pp. 2612-2620, 2012.

[20] M.A. Fnaiech, F. Betin, G.A. Capolino and F. Fnaiech, "Fuzzy logic and sliding-mode controls applied to six-phase induction machine with open phases," *IEEE Trans. Ind. Electron.*, vol. 57, no. 1, pp. 354-364, 2010.

[21] M. Barcaro, N. Bianchi and F. Magnussen, "Faulty operations of a PM fractional-slot machine with a dual three-phase winding," *IEEE Trans. Ind. Electron.*, vol. 58, no. 9, pp. 3825-3832, 2011.

[22] F. Meinguet, N. Ngac-Ky, P. Sandulescu, X. Kestelyn and E. Semail, "Fault-tolerant operation of an open-end winding five-phase PMSM drive with inverter faults," in *Proc. IEEE Ind. Elec. Soc. Annual Conf. IECON,* Vienna, Austria, pp. 5191-5196, 2013.

[23] S. Dwari and L. Parsa, "An optimal control technique for multiphase PM machines under open-circuit faults," *IEEE Trans. Ind. Electron.*, vol. 55, no. 5, 2008.

[24] S. Dwari and L. Parsa, "Fault-tolerant control of five-phase permanent-magnet motors with trapezoidal back EMF," *IEEE Trans. Ind. Electron.*, vol. 58, no. 2, pp. 476-485, 2011.

[25] A.S. Abdel-Khalik, A.S. Morsy, S. Ahmed and A.M. Massoud, "Effect of stator winding connection on performance of five-phase induction machines," *IEEE Trans. Ind. Electron.*, vol. 61, no. 1, pp. 3-19, 2014.

[26] I. Gonzalez, M.J. Duran, H.S. Che, E. Levi, and F. Barrero, "Fault-tolerant Control of Six-phase Induction Generators in Wind Energy Conversion Systems with Series-Parallel Machine-side Converters," *39th Annual Conference of the IEEE IES IECON2013*, Vienna (Austria), pp. 5274-5279, 2013.

[27] I. Gonzalez, M.J. Duran, H.S. Che, E. Levi and J.A. Aguado, "Fault-tolerant efficient control of six-phase induction generators in wind energy conversion systems with series-parallel machine-side converters," *in Proc. of Power Electronics, Machines and Drives Conf. PEMD*, Manchester, UK, CD-ROM, 2014.

[28] H.S. Che, E. Levi, M. Jones, M.J. Duran, W.P. Hew and N.A. Rahim, "Operation of a six-phase induction machine using series-connected machine-side converters," *IEEE Trans. Ind. Electron.*, vol.61, no. 1, pp. 164-176, 2014.

[29] H.S. Che, M.J. Duran, E. Levi, M. Jones, W.P. Hew and N.A. Rahim, "Postfault operation of an asymmetrical six-phase induction machine with single and two isolated neutral points," *IEEE Trans. Power Electron.*, vol. 29, no. 10, pp. 5406-5416, 2014.

[30] S.S. Gjerde, P.K. Olsen, K. Ljokelsoy and T.M. Undeland, "Control and fault handling in a modular series-connected converter for a transformerless 100 kV low-weight offshore wind turbine," *IEEE Trans. Ind. Appl.*, vol. 50, no. 2, pp. 1094-1105, 2014.

[31] X. Yuan, J. Chai, and Y. Li, "A transformer-less high-power converter for large permanent magnet wind generator systems," *IEEE Trans. Sustain. Energy*, vol. 3, no. 3, pp. 318-329, 2012.

[32] N. Bianchi, E. Fornasiero and S. Bolognani, "Thermal analysis of a five-phase motor under faulty operations," *IEEE Trans. Ind. Appl.*, vol. 49, no. 4, pp. 1531-1538, 2013.

[33] GAMS web, "A User's Guide", Available: http://gams.com/docs/

[34] A. Drud, "A GRG Code for Large Sparse Dynamic Nonlinear Optimization Problems," *Mathematical Programming*, vol. 31, pp. 153-191, 1985.

[35] A. Drud, "CONOPT-A Large Scale GRG Code," *ORSA Journal on Computing*, vol. 6, pp. 207-216, 1992.

[36] H. Guzmán, M.J. Duran, F. Barrero, L. Zarri, B. Bogado, I. González, M.R. Arahal, "Comparative Study of Predictive and Resonant Controllers in Fault-Tolerant Five-phase Induction Motor Drives," accepted for publication at *IEEE Trans. Ind. Electron.*, DOI: 10.1109/TIE.2015.2418732.

[37] H.S. Che, E. Levi, M. Jones, W.P. Hew and N.A. Rahim, "Current control methods for an asymmetrical six-phase induction motor drive," *IEEE Trans. Power Electron.*, vol. 29, no. 10, pp. 5406-5416, 2014.

[38] A. Yepes, J.A. Riveros, J. Doval-Gandoy, F. Barrero, O. Lopez, B. Bogado, M. Jones, E. Levi, "Parameter Identification of Multiphase Induction Machines with Distributed Windings-Part 1: Sinusoidal Excitation Methods," *IEEE Trans. Energy Convers.*, vol. 27, no. 4, pp. 1056-1066, 2012.

[39] J.A. Riveros, A. Yepes, F. Barrero, J. Doval-Gandoy, B. Bogado, O. Lopez, M. Jones, E. Levi, "Parameter Identification of Multiphase Induction Machines with Distributed Windings-Part 2: Time-Domain Techniques," *IEEE Trans. Energy Convers.*, vol. 27, no. 4, pp. 1067-1077, 2012.

Mario J. Duran was born in Málaga, Spain, in 1975. He received the M.Sc. and Ph.D. degrees in Electrical Engineering from the University of Málaga Spain, in 1999 and 2003, respectively. He is currently an Associate Professor with the Department of Electrical Engineering at the University of Málaga. His research interests include modeling and control of multiphase drives and renewable energies conversion systems.

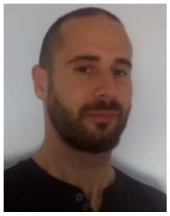

Ignacio Gonzalez Prieto was born in Malaga, Spain, in 1987. He received the Industrial Engineer and M. Sc. degrees from Univesity of Malaga, Spain, in 2012 and 2013, respectively. Currently, he is a PhD Student at the Department of Electronic Engineering in the University of Seville, Spain. His research interests include multiphase machines, wind energy systems and electrical vehicles.

Mario Bermudez was born in Málaga, Spain, in 1987. He received the Industrial Engineer degree from University of Málaga, Spain, in 2014. Currently, he is working toward the Ph.D. degree in the Electronic Engineering Department of the University of Seville, Spain. His current research interests include modeling and control of multiphase drives, DSP-based systems and electrical vehicles.

Federico Barrero (M 04; SM 05) received the MSc and PhD degrees in Electrical and Electronic Engineering from the University of Seville, Spain, in 1992 and 1998, respectively. In 1992, he joined the Electronic Engineering Department at the University of Seville, where he is currently an Associate Professor. He received the Best Paper Awards from the IEEE Trans. on Ind. Electron. for 2009 and from the IET Electric Power Applications for 2010-2011.

Hugo Guzman received the B.Eng. degree in Electronic Engineering from the Pontificia Universidad Javeriana, Bogotá-Colombia, in 2009 and MSc. Degree from the University of Seville, Spain in 2011. He joined the Electronic Engineering Department of the University of Seville in 2007 working as a research assistant from 2010-2012. He is currently a researcher at the University of Málaga.

Manuel R. Arahal (M'06) was born in Seville, Spain, in 1966. He received the M.Sc. and Ph. D. degrees in Electrical and Electronic Engineering from the University of Seville, Spain, in 1991 and 1996, respectively. From 1995 to 1998 he was an assistant professor and he is currently Full Professor with the Department of Systems Engineering and Automatic Control, University of Seville. His current research interests include model predictive control, artificial intelligence and forecasting techniques.